TURBULENCE AND SCALAR TRANSPORT IN HEATED BOUNDARY LAYERS WITH VISCOSITY STRATIFICATION

Jin Lee
Dept. of Mechanical Engineering
KAIST
291 Daehak-ro, Daejeon 305-701, Korea
Lee.Jin@kaist.ac.kr

Seo Yoon Jung
Advanced Reactor Development Institute
Korea Atomic Energy Research Institute
898-111, Daedeok-daero, Daejeon 305-353, Korea
syjung77@kaeri.re.kr

Hyung Jin Sung
Dept. of Mechanical Engineering
KAIST
291 Daehak-ro, Daejeon 305-701, Korea
hjsung@kaist.ac.kr

Tamer A. Zaki
Dept. of Mechanical Engineering
Imperial College London
Exhibition Road, London SW7 2AZ, UK
t.zaki@imperial.ac.uk

ABSTRACT

Direct numerical simulations (DNS) of turbulent boundary layers over isothermally-heated walls were performed to investigate the effect of viscosity stratification on the turbulent and thermal boundary layer flows. An empirical relation of temperature-dependent viscosity for water was adopted. Based on the free-stream temperature (30°C), two wall temperatures (70°C and 99°C) were selected. In the heated flows, the turbulence energy diminishes in the buffer layer, but increases near the wall. The reduction in turbulence kinetic energy in the buffer layer is accompanied by smaller levels of Reynolds shear stresses and, hence, weaker turbulence production. The enhanced turbulence energy near the wall is attributed to enhanced transfer of energy via additional diffusion-like terms due to the viscosity stratification. Wall heating also results in increased scalar flux in the sublayer. Large wall-normal gradients of U and Θ lead to increased production in the scalar flux budget.

Introduction

For water flows, the reduction of fluid viscosity can be readily achieved by wall heating, since the viscosity of common liquids decreases with increasing temperature. However, the effect of the gradual change in viscosity, i.e. viscosity stratification, on boundary layer turbulence is not clear. A number of studies in the literature were devoted to numerical simulations of turbulent thermal shear flows including, for example, the work of Kong et al. (2000) and Li (2011). These efforts have focused on scalar transport, and contributed to our understanding of turbulence structures including the velocity and temperature fluctuations in flows with various thermal boundary conditions and at different Prandtl numbers. Based on their direct numerical simulation of turbulent thermal boundary layers, Kong et al. (2000) demonstrated the similarity between wall-normal heat flux and the Reynolds stresses, which underlies the correlation between the temperature and the streamwise velocity perturbation fields.

Previous simulations have demonstrated that the scalar fluctuations and the scalar flux were increased with increasing Prandtl number. These studies have assumed constant fluid properties, in particular the fluid viscosity, or equivalently the Prandtl number. We herein relax this assumption and consider the case of temperature-dependent viscosity, where the Prandtl number varies spatially within the thermal boundary layer. One relevant study is the recent work by Zonta et al. (2012) who performed DNS of heated turbulent channel flow. They examined the effect of inhomogeneous viscosity and found that turbulence production and dissipation of the wall-bounded flow were dramatically changed. Their work did not, however, consider heating of spatially developing flows.

Therefore the present study aims to examine turbulence modification in response to wall heating of boundary layers with temperature-dependent viscosity. Direct numerical simulations are performed at two values of the wall temperature, $T_w = 70$°C and 99°C, which represent moderately heated (MH) and strongly heated (SH) walls. Note that the minimum viscosity above the heated wall is 50% of the free-stream value for the MH case and 35% for the SH case. For comparison, an isothermal configuration ($T_\infty = T_w = 30$°C), herein referred to as unheated wall (UH), was also simulated.

Simulation setup

In this study, the temperature-dependent viscosity of the fluid is defined according to the Arrhenius-type viscosity model for water (White, 2006):

$$\ln\left(\frac{\mu}{\mu_{ref}}\right) = a + b\left(\frac{T_{ref}}{T}\right) + c\left(\frac{T_{ref}}{T}\right)^2, \qquad (1)$$

where the curve-fit values are a=-2.10, b=-4.45 and c=6.55 corresponding to T_{ref}=273K and μ_{ref}=0.00179 kg/m·s. In order to quantify the effect of wall heating on viscosity variation only, density (ρ) and thermal diffusivity (α) were assumed to be constant as set by the free-stream temperature.

This assumption is appropriate for most common liquids, such as water, since changes in viscosity are much more significant than changes in density and in thermal diffusivity (Incropera and Dewitt, 1985). In effect, the current simulations address the forced convection problem, when the ratio of Grashof to the square of the Reynolds number is small, $Gr/Re^2 \ll 1$.

The Navier-Stokes, continuity and energy equations for an incompressible flow with temperature-dependent viscosity are written as:

$$\frac{\partial u_i}{\partial t}+u_j\frac{\partial u_i}{\partial x_j}=-\frac{\partial p}{\partial x_i}+\frac{1}{Re_{\theta_{in}}}\frac{\partial}{\partial x_j}\left[\nu_R\left(\frac{\partial u_i}{\partial x_j}+\frac{\partial u_j}{\partial x_i}\right)\right], \quad (2)$$

$$\frac{\partial u_i}{\partial x_i}=0, \quad (3) \qquad \frac{\partial \Theta}{\partial t}+u_j\frac{\partial \Theta}{\partial x_j}=\frac{1}{Re_{\theta_{in}}Pr}\frac{\partial^2\Theta}{\partial x_j^2}. \quad (4)$$

The velocity components in the streamwise (x), wall-normal (y) and spanwise (z) directions are u, v and w, respectively, and p is the pressure. The non-dimensionalized temperature is defined as Θ=(T-T_w)/(T_∞-T_w). Here, subscripts w and ∞ denote variables at the wall and in the free stream, respectively. The viscosity ratio ν_R is the ratio of the local to the free-stream viscosity, $\nu(T)/\nu_\infty$. The Reynolds number and Prandtl number in the governing equations are $Re_{\theta_{in}}(\equiv U_\infty\theta_{in}/\nu_\infty) = 1{,}240$ and $Pr(\equiv \nu_\infty/\alpha) = 5.4$, respectively. Here, α is the thermal diffusivity. The numerical method for the solution of the governing equations is summarized in Zaki *et al.* (2010), and was used previously for DNS of both transitional and turbulent boundary-layer flows.

In order to generate a realistic inflow for the main simulations, a precursor simulation of a transitional boundary layer was performed. The setup of the auxiliary computation is similar to the simulations by Jacobs and Durbin (2001). Instantaneous $y-z$ flow data were extracted sufficiently far downstream, at $Re_\theta = 1{,}240$, and applied as an inflow condition in the main TBL simulations. The parameters of the main simulations are summarized in table 1.

Table 1. Parameters of the direct numerical simulations.

	T_w[°C]	T_∞[°C]
Strongly heated (SH)	99	30
Moderately heated (MH)	70	30
Unheated (UH)	30	30

The size of the computational domain is L_x=400θ_{in}, L_y=60θ_{in} and L_z=80θ_{in}. The number of grid is 4097 × 385 × 1281 in all cases. Isothermal heating is applied downstream of the inlet. At the end of the streamwise domain, the Reynolds number of the unheated case reaches Re_θ =2,060. A non-uniform grid distribution is used in the wall-normal direction, whereas uniform grid spacing was used in the streamwise and the spanwise directions. The computational time step was $\Delta t = \{0.025,\ 0.018,\ 0.015\}\theta_{in}/U_\infty$ for the unheated (UH), the moderately heated (MH) and strongly heated (SH) cases, respectively, and the total averaging time was 1,800 θ_{in}/U$_\infty$. The simulations were carried out using 2,048 cores (HECToR Phase 3, Cray XE6, Interlagos).

The convective outflow condition $\partial u_i/\partial t + c\,\partial u_i/\partial x = 0$ was applied at the outlet of the main simulation, where c is the local bulk velocity. The no-slip condition was imposed at the bottom wall. Periodic boundary conditions were applied in the spanwise direction. At the top of the computational domain, the streamwise velocity was prescribed, $u = U_\infty$, and the wall-normal velocity was evaluated from the continuity equation, $v = -\frac{d}{dx}\int_0^{L_y} u\,\mathrm{d}y$.

In order to ascertain the reliability and accuracy of the simulations, the velocity statistics for the unheated case ($T_w = T_\infty$) are compared to the experimental data of Purtell et al. (1981) and the numerical data of Wu and Moin (2010). Good agreement with these datasets is demonstrated in figure 1(c). The mean scalar profile is compared to the correlation by Kader (1981) for boundary layers, and show favourable agreement (figure 2(a)). In addition, both the mean and the root-mean-square of the scalar are compared to the numerical simulations by Kawamura et al. (1998) for channel flow since data is not available for turbulent boundary layers at the same Prandtl number.

Turbulence statistics

The mean streamwise velocity normalized by U_∞ is shown in figure 1(a), at x/θ_{in}=275. At the same physical location, the mean velocity increases beneath $y/\delta \approx 0.4$ as wall-temperature increases. Near the boundary layer edge, the velocity is almost identical in all cases. This is qualitatively consistent with previous studies which describe an increase of the laminar base-flow velocity profile near the heated wall (Wall and Wilson, 1997). Turbulence intensities and Reynolds shear stress normalized by U_∞^2 are shown in figure 1(b). As the wall-temperature increases, all components of the turbulence intensity decrease in the buffer layer where the peak of $\overline{u'u'}$ is located, and all the way to the boundary layer edge. The wall-normal location of the peak position moves towards the wall. The trend of weaker turbulent fluctuations is prevalent in all the velocity components and in the Reynolds shear stress. However, as shown in the inset of figure 1(b), $\overline{u'u'}$ is increased in the near-wall region. This results from the downward shift of the peak position. The decreased Reynolds stresses are qualitatively consistent with results of turbulent channel flows with variable viscosity: Zonta et al. (2012) reported that the decreased turbulence intensities result from a stabilizing effect by the low viscosity near the heated wall.

The mean streamwise velocity is shown in figure 1(c) normalized by u_τ. It should be noted that here we adopt the modified inner length-scale, $l_\nu = \bar{\nu}(x,y)/u_\tau$, based on the local mean viscosity $\bar{\nu}(y)$ and the wall friction velocity. Whereas the length scale of the isothermal flow is constant, that of the heated flows decreases near the wall and increases away from the wall. Near the boundary layer edge ($y/\delta = 1$), the local viscosity is identical among all cases due to the thin thermal boundary layer thickness at high Pr. The standard law of the wall is also plotted in the figure. At the log-layer, when the wall is heated, the profiles are shifted upward from the unheated state with the same inclination angle. The intercept B increases, while the angle is identical. The thickness of the log-layer where the log-law is satisfied is almost unchanged in all cases. However, the

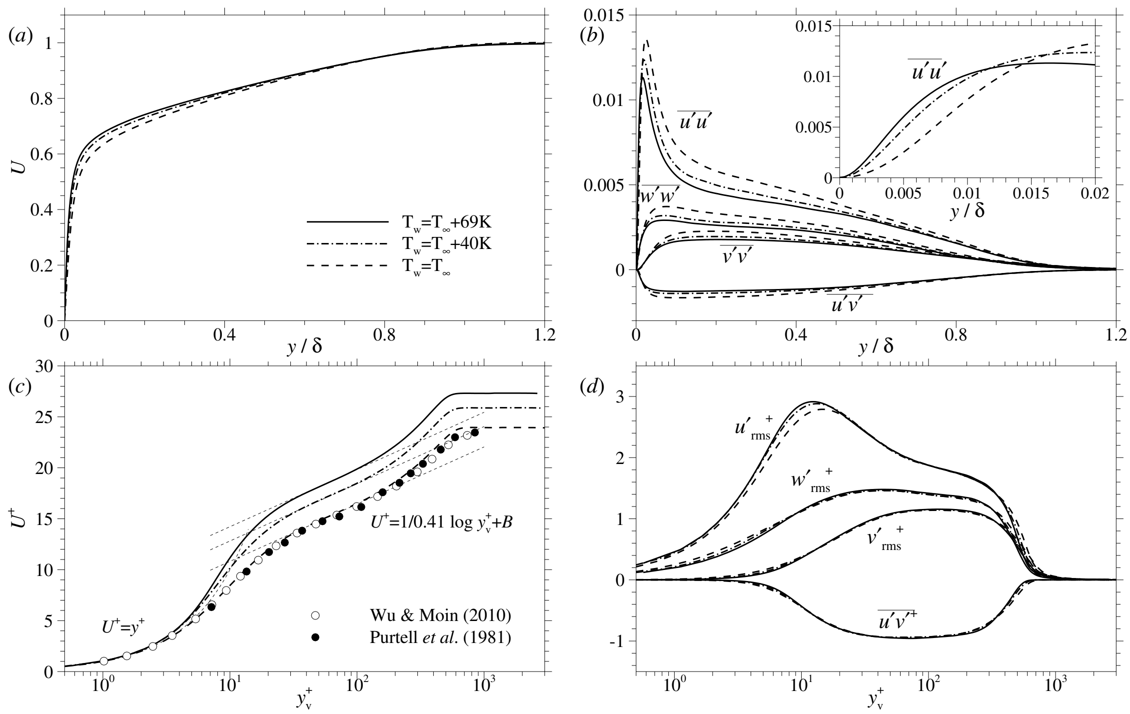

Figure 1. Profiles of (a) the mean streamwise velocity normalized by U_∞ and (b) variance of turbulence intensities and the Reynolds shear stress normalized by U_∞^2. Profiles of (c) the mean streamwise velocity and (d) root-mean-square (rms) of velocity fluctuations and the Reynolds shear stress normalized by u_τ. All profiles are drawn at x/θ_{in}=275 (Re$_\theta$=1,840 for $T_w = T_\infty$).

thickness of the sublayer where the linear law is satisfied is decreased with increasing wall temperature. Figure 1(d) shows the root-mean-square (rms) of the velocity fluctuations and the Reynolds shear stress. Although these quantities decreased based on outer scaling (figure 1(b)), they show better agreement regardless of the wall-temperature when normalized by u_τ. The agreement demonstrates that the modified inner lengthscale is the appropriate scaling.

The mean scalar profiles are shown in figure 2(a) normalized by the friction temperature, $\Theta_\tau \equiv -\frac{\alpha}{u_\tau}\left(\frac{\partial\overline{\Theta}}{\partial y}\right)_w$. The wall-normal position on the abscissa is normalized by the modified inner length-scale. The modified linear law for the mean scalar, which is defined by $\overline{\Theta}^+ = Pr(y)y_v^+$, is also plotted in the figure. Note that the local Prandtl number depends on the wall-normal distance due to viscosity stratification, unlike previous studies of passive scalar transport in isothermal turbulent boundary layers. Thus, as the fluid temperature is increased due to proximity to the heated wall, $Pr(y)$ is decreased and the mean scalar is reduced. In addition, the mean scalar profile is decreased throughout the boundary layer due to the higher friction temperature (Li, 2011). This accounts for the lower scalar profile in the wake region for the heated flows, even though $Pr(y)$ has reached the reference value. The rms of the scalar fluctuation is shown in figure 2(b). Similar to the mean scalar profile, increasing the wall temperature results in a decrease in the rms of the scalar fluctuations.

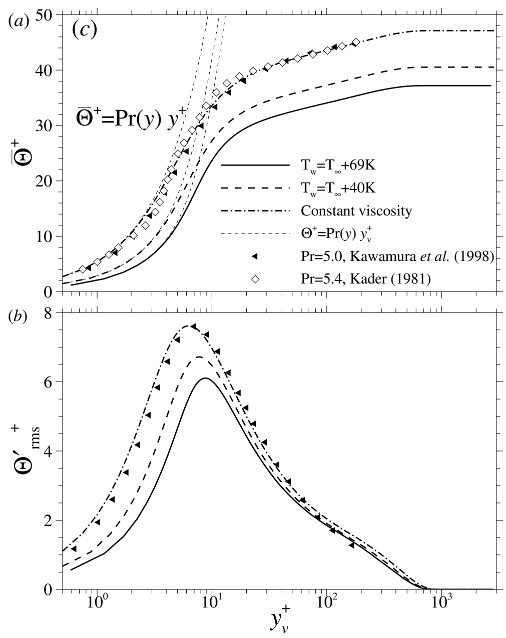

Figure 2. Wall-normal distribution of (a) mean scalar and (b) root-mean-square (rms) of scalar fluctuation at x/θ_{in}=275 (Re$_\theta$=1,840 for $T_w = T_\infty$). Each profiles are normalized by the friction temperature.

Turbulence kinetic energy budget

Statistical analysis of DNS data yields all the terms in the budget for the turbulence kinetic energy (TKE) explicitly. Such analysis can clarify the dynamical characteristics of turbulence, for example the production, redistribution and dissipation of TKE. Since the viscosity is not constant in the momentum equation, additional terms related to the viscosity gradient and fluctuations must be evaluated. The TKE equation for temperature-dependent viscosity is

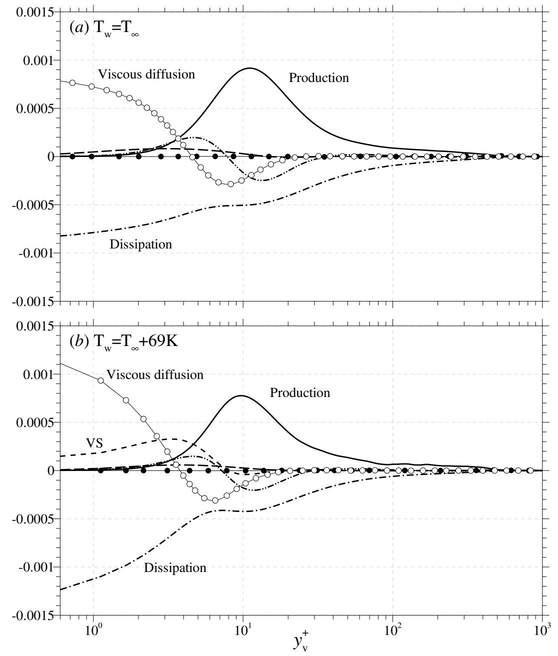

Figure 3. Budgets of turbulent kinetic energy for (a) $T_w = T_\infty$ (UH) and (b) $T_w = T_\infty + 69K$ (SH) at Re_θ^{eff}=1,840. Every terms are normalized by U_∞^3/θ_{in}. ——, production; – – –, dissipation; – – –, sum of the VS terms; — —, pressure diffusion; – - - –, turbulent transport; —●—, convection; —○—, viscous diffusion.

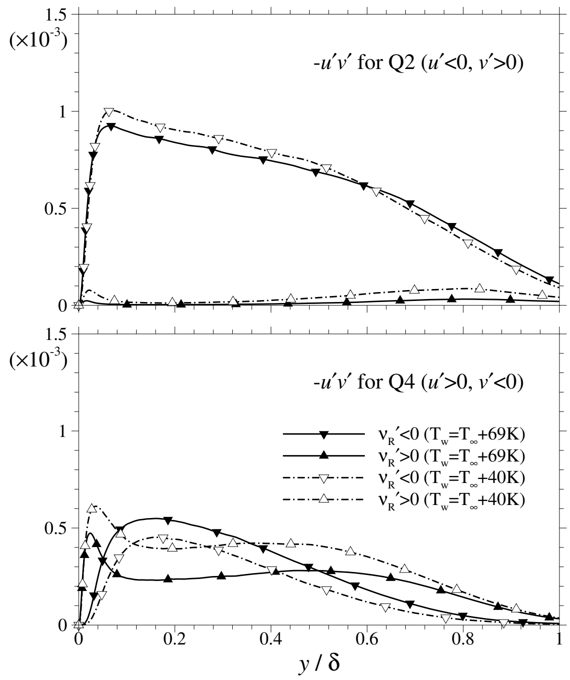

Figure 4. Profiles of the Q2 (top) and Q4 (bottom) events with viscosity fluctuation (ν') of the Reynolds shear stress ($-\overline{u'v'}$) at Re_θ^{eff}=1,840. Each profiles are normalized by the free-stream velocity.

given below:

$$\frac{\partial}{\partial t}\left(\frac{1}{2}\overline{u_i'u_i'}\right) + C = P + \Pi + G + T + D + \varepsilon + VS, \quad (3)$$

where C is convection by the mean flow, P is production, $\Pi + G$ is velocity–pressure-gradient correlation, T is turbulent transport, D is viscous diffusion due to the mean viscosity profile and ε is dissipation (Pope, 2000). We have herein decomposed the viscous diffusion and dissipation terms into the contributions due to the effective viscosity, D and ε respectively, and all other contributions due to viscosity stratification. The latter terms are lumped into the term VS (for details, see Lee et al., 2013). The budget for the TKE, $k \equiv \frac{1}{2}\langle u_i u_i\rangle$, is shown in figure 3, normalized by U_∞^3/θ_{in}. Statistical convergence was verified by ensuring that $\frac{\partial}{\partial t}\left(\frac{1}{2}\overline{u_i'u_i'}\right)$ was two orders of magnitude smaller than the leading terms in the budget.

In the case of wall heating, the peak value of the production is reduced and its wall-normal position also decreases. Since both the mean-shear rate and Reynolds-shear-stress in the buffer region are reduced for the heated wall, the reduced production is inevitable. Despite the decrease in the mean viscosity near the wall, the magnitude of the dissipation term is increased in the case of wall heating. It is evident from figure 3 that the magnitude of ε is rather significantly increased for the heated wall. While viscous diffusion is balanced by the dissipation at the wall for the UH case, in the heated flow the dissipation balances the sum of viscous diffusion and the additional VS terms. Above the viscous sublayer ($y_v^+ > 5$), the dissipation term of the heated flow becomes smaller than that of the unheated case.

Since the magnitudes of the dissipation and the production are most dominant relative to the other terms within the viscous sublayer and in the buffer layer, respectively, the kinetic energy produced in the buffer layer is transported to the sublayer to maintain the energy balance (Pope, 2000). The larger dissipation of the heated flow is consistent with a more pronounced energy transfer, in comparison to the unheated case. As a result, figure 3(b) shows enhanced viscous diffusion in addition to the newly derived additional VS term. The VS term is the second largest gain in the viscous sublayer. Furthermore, the VS term is negative (loss) near the production peak and is positive (gain) in the sublayer. Therefore, the VS term transports TKE towards the wall similar to viscous diffusion due to the effective viscosity.

Reynolds shear stress: ejections and sweeps

In addition to the streamwise and wall-normal velocity fluctuations, the influence of viscosity fluctuations is also considered in terms of contribution to the Reynolds shear stress. The octant analysis for the Reynolds shear stress is presented in figure 4, which shows contribution to the Reynolds shear stress divided by the sign of u', v' and ν_R'. Since Q1 and Q3 events remain inappreciably affected by heating, only Q2 and Q4 events of the heated cases ($T_w = T_\infty + 40K$ and $T_w = T_\infty + 69K$) are shown in figure 4.

Since a lower-viscosity fluid is established near the hot wall, it is conceivable that ejection events are mostly associated with the upwards displacement of low-viscosity (hot) fluid. This is illustrated in figure 4 where Q2 events consist predominantly of the contribution due to low-viscosity (hot) fluid motion. In the case of Q4 events, contributions of both high- and low-viscosity fluid appear important. The former are intuitive, and can be attributed to sweeps of outer fluid ($y/\delta > 0.5$ for the SH case). On the other hand, the dis-

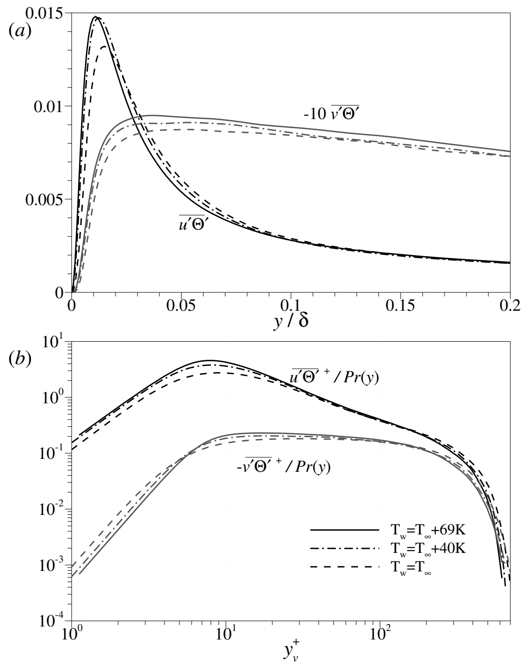

Figure 5. Profiles of the scalar flux, $\overline{u_i'\Theta'}$, at $Re_\theta^{eff} = 1,840$ normalized by (a) the outer length scale and (b) the inner length scale. The normalization in (b) uses the local Prandtl number, $Pr(y)$.

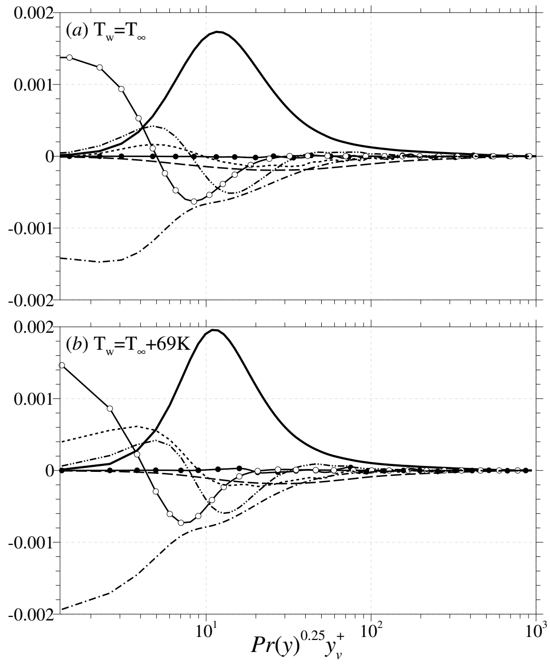

Figure 6. Budgets of scalar flux $\overline{u'\Theta'}$ for (a) $T_w = T_\infty$ (UH) and (b) $T_w = T_\infty + 69K$ (SH) at Re_θ^{eff}=1,840. Every term is normalized by U_∞^3/θ_{in}. ——, production; – – –, dissipation; — —, pressure diffusion; – - – -, turbulent transport; —•—, convection; —◦—, viscous diffusion; - - -, $\partial\left(\overline{u'\Theta'}\right)/\partial t + VS_{\Theta i}$.

placement of low-viscosity fluid towards the heated surface must be carefully interpreted. These events are identified as $\nu_R' < 0$ relative to the mean, or effective, viscosity which is a smooth function in the wall-normal coordinate. Therefore, they represent sweeps of instantaneously hotter fluid than the mean. The net effect of wall heating on Q4 events is an overall reduction in the contribution to Reynolds stress.

Thermal transport

In simulations of passive scalar transport, the velocity field is unaffected by temperature. However, as shown in the previous section, the velocity field of practical liquids is changed owing to temperature gradients, via the changes in viscosity. This can lead to changes in the scalar flux ($\overline{u_i'\Theta'}$). Note that the computation of the scalar field assumed constant thermal diffusivity (α). In this section, the variation of the scalar flux owing to the temperature-dependent viscosity is investigated.

Profiles of scalar flux, $\overline{u_i'\Theta'}$, are shown in figure 5. In the outer scaling (figure 5(a)), both the streamwise and wall-normal scalar fluxes are increased near the heated wall. The profile of the streamwise scalar flux is essentially similar to the streamwise velocity fluctuation shown in the inset of figure 1(b). In the log-log plot (figure 5(b)), the profiles are normalized by $Pr(y)$ and show a linear dependence on y_v^+ near the wall. The near-wall slope is 2 and 3 for $\overline{u'\Theta'}$ and $\overline{v'\Theta'}$, respectively, which is the same as that observed at constant viscosity, i.e. constant Pr, (Kong et al., 2000). Although the near-wall slope is identical irrespective to the wall temperature, the near-wall value of $\overline{u'\Theta'}$ ($\overline{v'\Theta'}$) slightly increases (decreases) as the wall-temperature increases. Unlike conventional simulations of the passive-scalar transport, the present study shows variation of the scalar flux due to the temperature-dependent viscosity. This implies that results from the passive-scalar transport could be dissimilar to real fluids with large temperature gradients.

The transport equation for the scalar flux is given below (Li, 2011):

$$\frac{\partial\left(\overline{u_i'\Theta'}\right)}{\partial t} + C_{\Theta i} = P_{\Theta i} + \Pi_{\Theta i} + G_{\Theta i} + T_{\Theta i} + D_{\Theta i} + \varepsilon_{\Theta i} + VS_{\Theta i}. \tag{4}$$

The term $VS_{\Theta i}$ denotes the sum of all additional terms owing to the temperature-dependent viscosity. Physical meaning of each term in the transport equation is the same as in equation 3. Profiles of the scalar flux budget for $\overline{u'\Theta'}$ are shown in figure 6. The budget of the wall-normal scalar flux, $\overline{v'\Theta'}$, is not shown but is similar. The scaling of the wall-normal coordinate by Li (2011) ($Pr^{0.25}y^+$) is modified to take into account the local Pr, i.e. $Pr(y)^{0.25}y_v^+$. In order to compare the effect of wall heating from identical upstream condition, all terms are normalized by U_∞^2/θ_{in}. Here it should be noted that the dotted line in figure 6 is the sum of the time derivative ($\partial(\overline{u'\Theta'})/\partial t$) and the $VS_{\Theta i}$ term. Since the time derivative should be zero in all cases, the dotted line is mostly due to the additional $VS_{\Theta i}$ term. Similarly to the TKE budget, the production term and the viscous diffusion terms are the largest in the buffer layer and the viscous sublayer, respectively. The peak value of the production is increased for the heated flow. Here, the production term for $\overline{u'\Theta'}$ is:

$$P_{\Theta 1} = -\overline{u'\Theta'}\frac{\partial U}{\partial x} - \overline{v'\Theta'}\frac{\partial U}{\partial y} - \overline{u'u'}\frac{\partial \Theta}{\partial x} - \overline{u'v'}\frac{\partial \Theta}{\partial y}. \tag{5}$$

The increase of the peak value results from the 2nd and 4th terms in equation (5), since the remaining terms are negligible given the relatively small value of the mean streamwise gradients in comparison to the wall-normal gradients. Even though values of $-\overline{v'\Theta'}$ and $-\overline{u'v'}$ are only slightly changed in the sublayer and the buffer region for the heated flow, those of $\partial U/\partial y$ and $\partial \Theta/\partial y$ are largely increased in these regions. The increased wall-normal gradients are mainly responsible for the large production in the heated flow. In the meantime, the viscous diffusion term is decreased and the dissipation term is increased near the wall in the heated flow. The changes in the viscous diffusion and the dissipation are compensated by the $VS_{\Theta i}$ term. The rest of the terms remain largely unchanged in the case of temperature-dependent viscosity.

Summary and conclusions

Direct numerical simulations of turbulent boundary layers with temperature-dependent viscosity were performed to investigate the influence of wall-heating on boundary layer flows. The fluid viscosity model was chosen to represent water, i.e. lower viscosity at higher temperature, at atmospheric pressure. Based on the free-stream temperature of 30°C, two wall temperatures (70°C and 99°C) were considered.

Profiles of velocity and scalar fields were presented scaled by the modified inner length scale for the inhomogeneous viscosity. The log-law of the mean streamwise velocity profile was shifted upward. The turbulence intensity and the Reynolds shear stress were decreased in the heated flows. In addition, both the mean scalar and scalar fluctuation were reduced in the heated flows relative to the constant viscosity configuration. The budget of the turbulent kinetic energy demonstrated that the production term was weakened in the heated flow, owing to the weaker Reynolds shear stress. On the other hand, the near-wall dissipation was increased despite the lower viscosity near the wall. In addition, terms due to viscosity stratification were shown to have an effect similar to viscous diffusion. It was concluded that viscosity stratification leads to larger energy transfer towards the wall from the buffer region, as compared to the flow over the unheated wall.

The budget of the streamwise scalar flux showed that the peak value of the production is increased for the heated wall. The large wall-normal gradients of the mean streamwise velocity and the mean scalar were mainly responsible for the large production of the scalar flux in the heated flow.

The authors would like to acknowledge the financial support from the Creative Research Initiatives (No. 2013-003364) programme of the National Research Foundation, Korea and the European Commission through the Erasmus Mundus Build on Euro-Asian Mobility (EM-BEAM) programme. We are also grateful for the financial and computing (HECToR) support from the UK Engineering and Physical Sciences Research Council (EPSRC).

REFERENCES

Incropera, F. P. & Dewitt, D. P. 1985 Fundamentals of heat and mass transfer. John Wiley and Sons.

Jacobs,R. G. & Durbin, P. A. 2001 Simulations of bypass transition. *Journal of Fluid Mechanics* **428**, 185–212.

Kader, B.A. 1981 Temperature and concentration profiles in fully-turbulent boundary layers. *International Journal of Heat and Mass Transfer* **24**, 1541–1544.

Kawamura, H., Ohsaka, K., Abe, H. & Yamamoto, K. 1998 DNS of turbulent heat transfer in channel flow with low to medium-high Prandtl number fluid. *International Journal of Heat and Fluid Flow* **19**, 482–491.

Kong, H., Choi, H. & Lee. J. S. 2000 Direct numerical simulation of turbulent thermal boundary layers. *Physics of Fluids* **12**, 2555–2568.

Lee, J., Jung, S.Y., Sung, H.J. & Zaki, T.A. 2013 Effect of wall heating on turbulent boundary layers with temperature-dependent viscosity. *Journal of Fluid Mechanics* – In press.

Li, Q. 2011 Direct and large-eddy simulations of turbulent boundary layers with heat transfer. PhD thesis, Royal Institute of Technology (KTH), Stockholm, Sweden.

Pope, S. B. 2000 Turbulent flows. Cambridge University Press.

Purtell, L. P., Klebanoff, P. S. and Buckley, F. T. 1981 Turbulent boundary layer at low Reynolds number. *Physics of Fluids* **24**, 802–811.

Tiselj, I., Pogrebnyak, E., Li, C., Mosyak, A., & Hetsroni, G. 2001 Effect of wall boundary condition on scalar transfer in a fully developed turbulent flume. *Physics of Fluids* **13**, 1028–1039.

Wall, D. P. & Wilson, S. K. 1997 The linear stability of flat-plate boundary-layer flow of fluid with temperature-dependent viscosity. *Physics of Fluids* **9**, 2885–2898.

White, F. M. 2006 Viscous fluid flow (third edition). McGraw-Hill.

Wu, X. & Moin, P. 2010 Transitional and turbulent boundary layer with heat transfer. *Physics of Fluids* **22**, 085105.

Zaki, T. A., Wissink, J. G., Rodi, W., & Durbin, P. A. 2010 Direct numerical simulations of transition in a compressor cascade: the influence of free-stream turbulence. *Journal of Fluid Mechanics* **665**, 57–98.

Zonta, F., Marchioli, C. & Soldati, A. 2012 Modulation of turbulence in forced convection by temperature-dependent viscosity. *Journal of Fluid Mechanics* **697**, 150–174.